Cyclic Deformation Behavior of a Transformation-Induced Plasticity–Aided Dual-Phase Steel

KOH-ICHI SUGIMOTO, MITSUYUKI KOBAYASHI, and SHIN-ICHI YASUKI

Cyclic hardening-softening behavior of a *TRIP-aided dual-phase* (TDP) *steel* composed of a ferrite matrix and retained austenite plus bainite second phase was examined at temperatures ranging from 20 °C to 200 °C. An increment of the cyclic hardening was related to (1) a long-range internal stress due to the second phase and (2) the strain-induced transformation (SIT) behavior of the retained austenite, as follows. Large cyclic hardening, similar to a conventional ferrite-martensite dual-phase steel, appeared in the TDP steel deformed at 20 °C, where the SIT of the retained austenite occurred at an early stage. This was mainly caused by a large increase in strain-induced martensite content or *strain-induced martensite hardening*, with a small contribution of the internal stress. In this case, shear and expansion strains on the SIT considerably decreased the internal stress in the matrix. With increasing deformation temperature or retained austenite stability, the amount of cyclic hardening decreased with a significant decrease in plastic strain amplitude. This interesting cyclic behavior was principally ascribed to the internal stress, which was enhanced by stable and strain-hardened retained austenite particles.

I. INTRODUCTION

Recently, a new type of 600 to 1000 MPa grade high-strength dual-phase sheet steel composed of a ferrite matrix and second phase (bainite plus retained austenite) was developed for the purpose of weight reduction of various automotive structural press parts.[1–7] The steel, which is named *TRIP-aided dual-phase* (TDP) steel, has excellent press formability associated with the transformation-induced plasticity (TRIP)[8] of the retained austenite, since the martensite-start temperature M_s is somewhat lower than room temperature, *i.e.*, between 0 °C and −100 °C.[2,3,4] So, many studies[2–8] on the formability have been conducted to apply the TDP steel to automotive underbody parts such as suspension arms and wheel disks.

The underbody press parts are subjected to severe cyclic loading below or above yielding stress, so that high fatigue strength may be required, as well as further improvement of formability. However, there are a few basic findings[9] on TDP fatigue properties.

In general, monotonic deformation of the TDP steel is controlled by the following two items:

(1) long-range internal stress resulting from a difference of plastic strain between the ferrite matrix and the second phase;[10,11] and
(2) strain-induced transformation (SIT) of the retained austenite resulting in both the increases in strain-induced martensite content and the relaxation of the long-range internal stress.

These items are influenced by retained austenite stability, which is controlled by retained austenite parameters (carbon concentration and morphology) and deformation conditions (temperature, strain rate, and state of stress).[2–6,10,11]

If the retained austenite is stable against straining, then the retained austenite particle, as a hard phase, effectively enhances the internal stress during early stages.[10,11] The stable retained austenite tends to transform to martensite over a large strain range, thereby resulting in extremely large elongations by TRIP effects.[2,3,4] On the other hand, if the retained austenite is unstable, most of the retained austenite particles transform to martensite at an early stage. The resultant strain-induced martensite considerably increases the flow stress with relatively low elongations and relaxed internal stress.[10,11]

The internal stress during early stages is assumed to play an important role in fatigue properties of the TDP steel, as well as the increased martensite content. In the present work, to understand the basic fatigue property of the TDP steel, cyclic hardening-softening behavior and the internal stress were examined at temperatures ranging from 20 °C to 200 °C, where the SIT behavior considerably varies. And, the cyclic hardening-softening behavior was related to the SIT behavior and the internal stress.

II. EXPERIMENTAL PROCEDURE

In the present study, the TDP and DP steel bars of composition shown in Table I were prepared as a vacuum-melted 100-kg ingot followed by hot forging and subsequently hot rolling to 13 mm in diameter. After machining tensile and cyclic specimens of 10-mm gage length by 7-mm diameter, the TDP specimens were subjected to intercritical annealing (or annealing in $\alpha + \gamma$ region) at 780 °C for 1200 seconds followed by austempering at 400 °C for 1000 seconds. The intercritical annealing temperature corresponds to where the retained austenite volume fraction becomes maximum.[3] The DP specimens were intercritically annealed at 780 °C for 1200 seconds followed by oil quenching to obtain a ferrite-martensite dual-phase structure without retained austenite.

KOH-ICHI SUGIMOTO, Associate Professor, and MITSUYUKI KOBAYASHI, Professor, are with the Department of Mechanical Systems Engineering, Shinshu University, Nagano 380, Japan. SHIN-ICHI YASUKI, formerly Graduate Student, Department of Mechanical Systems Engineering, Shinshu University, is Metallurgical Engineer with Steel Wire Rod and Bar Development, Kobe Works, Kobe Steel Ltd., Kobe 657, Japan.

Manuscript submitted August 19, 1996.

Table I. Chemical Composition of Steels Used (Mass Percent)

Steel	C	Si	Mn	P	S	Al
TDP	0.20	1.50	1.50	0.015	0.0012	0.041
DP	0.13	1.01	1.01	0.003	0.0010	0.022

Table II. X-ray Measurement Conditions and Material Constants

Phase	α	γ
Characteristic X-ray	Cr K_α	
Filter	Vanadium	
Voltage, current	40 kV − 30 mA	
Slit, irradiation mask	0.5 deg, 5 × 8 mm²	
Scanning speed	1 deg/min	
ψ	10, 20, 30, 40, 45 deg	
Diffraction plane	(211)	(220)
Young's modulus	223 GPa	192 GPa
Poisson's ratio	0.28	0.28

Tensile and cyclic tests were carried out using an Instron type of tensile testing machine. Tension-compression cyclic testing was done under constant strain amplitude of $\Delta\varepsilon = \pm 1.0$ or ± 2.0 pct at 20 °C, 100 °C, and 200 °C and at a crosshead speed of 1 mm/min. The hysteresis curves were recorded during every cycle.

The amount of retained austenite was quantified by X-ray diffractometry using Mo K_α radiation. To minimize the effect of texture, the volume fraction of retained austenite was quantified on the basis of the integrated intensity of $(200)_\alpha$, $(211)_\alpha$, $(200)_\gamma$, $(220)_\gamma$, and $(311)_\gamma$ diffraction peaks, termed the five-peak method.[12] The retained austenite lattice parameter $a_{\gamma 0}$ was measured from the $(220)_\gamma$ diffraction peak using Cr K_α radiation[3] on the electrochemically polished surface of as-austempered TDP steel, where there is negligible internal stress. From the measured $a_{\gamma 0}$ value (10^{-10} m) and the following equation,[13] an initial carbon concentration of the retained austenite particles $C_{\gamma 0}$ (mass pct) was calculated.

$$\alpha_{\gamma 0} = 3.5467 + 0.0467 C_{\gamma 0} \qquad [1]$$

The M_s (°C) of retained austenite was estimated by substituting the $C_{\gamma 0}$ value into the following equation:

$$M_s = 550 - 360 \times C_{\gamma 0} - 40 \times Mn_{\gamma 0} \qquad [2]$$

where the manganese concentration ($Mn_{\gamma 0}$, mass pct) in the retained austenite was estimated to be 1.5 times the manganese content by Speich *et al.*[14]

The 2θ-$\sin^2\psi$ method[15] was applied to X-ray studies of internal stress σ_x. Namely, variations in 2θ with $\sin^2\psi$ were measured with respect to $(211)_\alpha$ and $(220)_\gamma$ diffraction peaks using Cr K_α radiation. Then, the slope ($d2\theta / d\sin^2\psi$) was substituted in the following equation:

$$\sigma_X = -\{E/2(1+\nu)\} \cot\theta_0 \, (d2\theta/d\sin^2\psi) \qquad [3]$$

where θ_0 and θ represent diffraction angles under free strain and on straining, respectively. The term ψ is an angle between the reflecting-plane normal and surface normal. The terms E and ν are the Young's modulus and Poisson's ratio of each phase, respectively. The measurement conditions and material constants in Eq. [3] are shown in Table II. In the present study, the $(211)_\alpha$ peak corresponds to that of the body-centered cubic phase composed of the ferrite matrix (α_f), the bainite (α_b), and the strain-induced martensite (α_m).

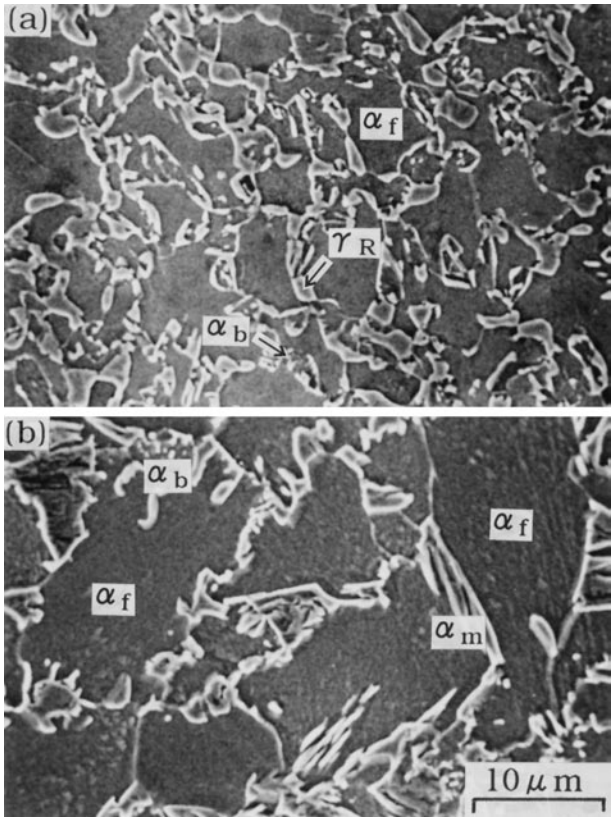

Fig. 1—Scanning electron micrographs of (*a*) as-austempered TDP steel and (*b*) as-intercritically annealed DP steel, in which α_f, α_B, α_m, and γ_R represent ferrite matrix, bainite, martensite, and retained austenite, respectively.

To clarify the deformation-transformation behavior of retained austenite particles, thin foils of the specimens cyclically deformed were observed in a JEOL*-4000EX transmission electron microscope. In addition, the line breadth at a half-maximum X-ray intensity $\Delta\theta_x$, which corresponds to plastic strain and dislocation density, was measured from the $(220)_\gamma$ diffraction peak using Cr K_α radiation.

*JEOL is a trademark of Japan Electron Optics Ltd., Tokyo.

III. RESULTS

A. *Microstructure and Tensile Properties*

Figure 1 shows scanning electron micrographs of (a) as-austempered TDP steel and (b) as-intercritically annealed DP steel. Metallurgical parameters of the TDP and the DP steels are shown in Table III. The microstructure of the TDP steel is composed of the ferrite matrix and 30 vol pct hard second phase (13 vol pct stable retained austenite particles plus 17 vol pct bainite islands) along the ferrite grain boundaries. Most of the retained austenite particles, whose mean size is less than 2 to 3 μm, are isolated from or adjacent to the bainite islands. The DP steel used for comparison has the same second-phase morphology as the TDP steel. However, the second phase consists of marten-

Table III. Metallurgical Parameters of Steels Used

Steel	f (Vol Pct)	$f_{\gamma 0}$ (Vol Pct)	$\alpha_{\gamma 0}$ ($\times 10^{-10}$ m)	$C_{\gamma 0}$ (Mass Pct)	M_s (°C)
TDP	0.30	0.13	3.6116	1.390	−40.4
DP	0.28	0.0	—	—	—

Note: f: volume fraction of the second phase, $f_{\gamma 0}$: initial volume fraction of the retained austenite, $\alpha_{\gamma 0}$: initial lattice parameter of the retained austenite, $C_{\gamma 0}$: initial carbon concentration of the retained austenite, and M_s: martensite-start temperature of the retained austenite.

Table IV. Tensile Properties at 20 °C, 100 °C, and 200 °C in TDP and DP Steels Used

Steel	T (°C)	YS (MPa)	UTS (MPa)	UEl (Pct)	TEl (Pct)	RA (Pct)
	20	470	820	29	52	60
TDP	100	437	724	35	59	65
	200	433	694	40	61	62
	20	273	717	20	43	57
DP	100	299	681	23	44	57
	200	325	696	22	38	55

T: testing temperature, YS: yielding stress, UTS: ultimate tensile strength, UEl: uniform elongation, TEl: total elongation, and RA: reduction of area.

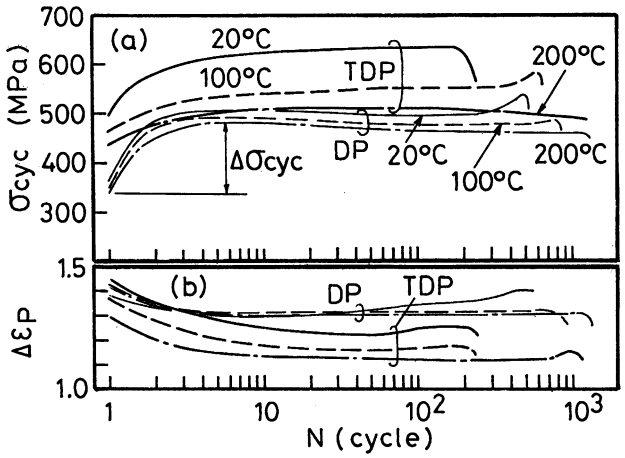

Fig. 2—Variations in (*a*) stress amplitude σ_{cyc} and (*b*) plastic strain amplitude $\Delta\varepsilon_P$ with number of cycles for TDP and DP steels cyclically deformed at 20 °C, 100 °C and 200 °C ($\Delta\varepsilon = \pm 1$ pct).

site islands mixed with a small amount of bainite, differing from that of the TDP steel. Furthermore, the DP steel has a larger ferrite grain size than the TDP steel.

Table IV shows the tensile properties of both the steels at various deformation temperatures. Large increases in elongation are obtained only in the TDP steel deformed at 100 °C and 200 °C, with a concomitant decrease in tensile strength. According to a previous study,[4] these temperatures (100 °C and 200 °C) agree with the temperatures at which the retained austenite becomes the most stable against the SIT.

B. *Cyclic Hardening-Softening Behavior*

Figure 2(a) shows the variation in stress amplitude σ_{cyc} with the number of cycles N under $\Delta\varepsilon = \pm 1$ pct for the TDP and the DP steels. And, Figure 3 shows the $\sigma_{cyc} -$

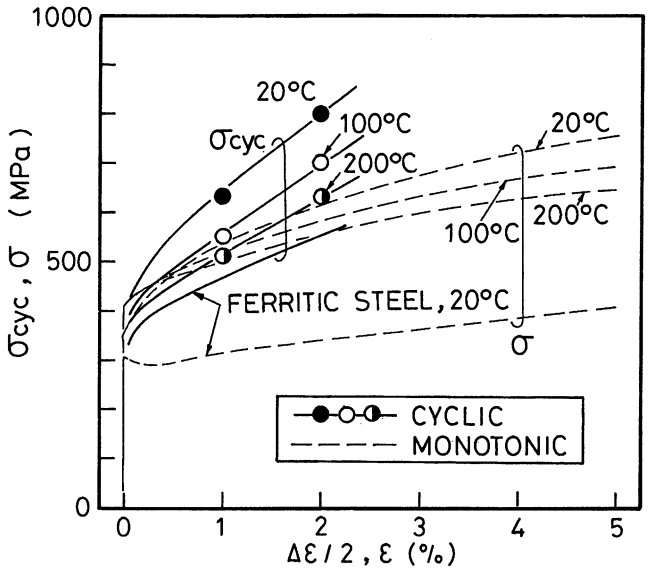

Fig. 3—Stress-strain (σ-ε) curves on monotonic deformation and stress amplitude at $N = N_f/2$; a half-strain amplitude (σ_{cyc}-$\Delta\varepsilon/2$) curves on cyclic deformation at various temperatures for TDP and 0.006C-1.50Si-1.50Mn-0.036Al (mass pct) ferritic steels.[9]

$\Delta\varepsilon/2$ curves at a steady state, *i.e.*, at a half-cycle number to fracture $N = N_f/2$, in the TDP steel. Large cyclic hardening, which is characterized by the rapid hardening at the early stage and the subsequent moderate hardening or small softening at the later stages, appears in TDP steel, similar to that of the DP steel. Such a cyclic hardening behavior considerably differs from those of the precipitation-hardening steel and the martensitic steel, which undergo a typical cyclic softening.[16] If the cyclic hardening increment $\Delta\sigma_{cyc}$ is defined by a difference in σ_{cyc} between at the $N = 1$ cycle and at the given cycles, as shown in Figure 2, the $\Delta\sigma_{cyc}$ of the TDP steel cyclically deformed to $N = N_f/2$ cycles at 20 °C is nearly equal to that of the DP steel.

The σ_{cyc} of the TDP steel reduces gradually with increasing deformation temperature, accompanied with a decrease in the $\Delta\sigma_{cyc}$. Such a significant temperature dependence of the cyclic hardening behavior hardly appears in the DP steel.

Figure 4 shows hysteresis curves (a) at $N = 1 \rightarrow 2$ cycles and (b) at $N = 10 \rightarrow 11$ cycles for the TDP and the DP steels. From this figure and Figure 2(b), it is found that the plastic strain amplitude $\Delta\varepsilon_p$ of the TDP steel is considerably reduced at 100 °C and 200 °C. This interesting behavior results from a decrease in the apparent Young's modulus and/or an initial flow stress on reverse deformation. The reason for this will be discussed in section IV.C.

C. *X-ray Internal Stress*

Figure 5 shows a typical 2θ-$\sin^2\psi$ plot obtained from $(220)_\gamma$ and $(211)_\alpha$ diffraction peaks in as-annealed or cyclically deformed TDP steel. Since the 2θ-$\sin^2\psi$ relation is linear, these X-ray internal stresses can be accurately calculated by substituting the slope $d2\theta/\mathrm{d}\sin^2\psi$ into Eq. [3].

Figure 6 shows the X-ray internal stresses in a longitudinal direction of retained austenite particles $\sigma_{X\gamma}$ and body-centered cubic phase $\sigma_{X\alpha}$ in the present TDP steel, which is cyclically deformed to $N = N_f/2$ cycles under $\Delta\varepsilon/2$ or

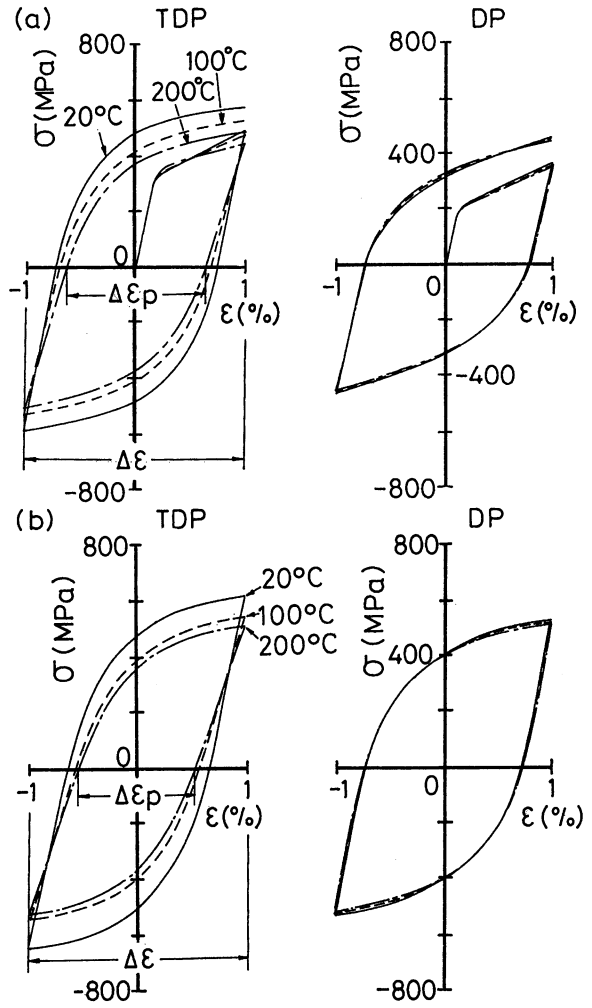

Fig. 4—Changes in hysteresis curves at (*a*) $N = 1 \rightarrow 2$ and (*b*) $N = 10 \rightarrow 11$ cycles with deformation temperature for TDP and DP steels.

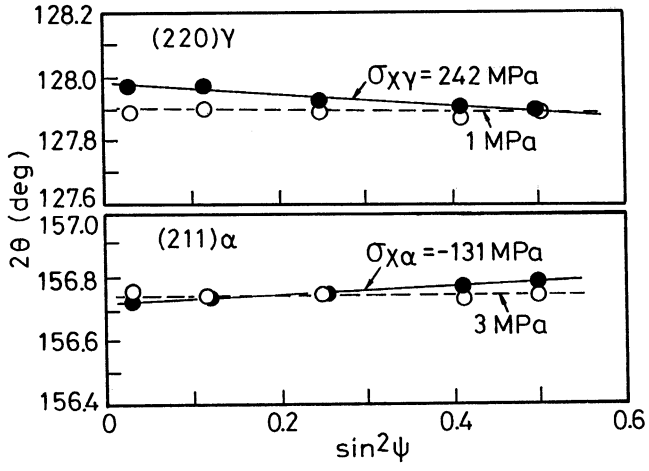

Fig. 5—2θ-$\sin^2\psi$ plot measured from $(220)_\gamma$ and $(211)_\alpha$ diffraction peaks of steels cyclically deformed to $N = N_f/2$ cycles at 200 °C and $\Delta\varepsilon/2 = 1$ pct (●) or annealed (○).

monotonically deformed to ε. When compared with monotonic deformation, higher positive or tensile internal stress is found to occur in untransformed retained austenite regions and particles during cyclic deformation. The internal stress considerably increases with increasing testing temperature, despite the decreased stress amplitude σ_{cyc} (Figures 2 through 4).

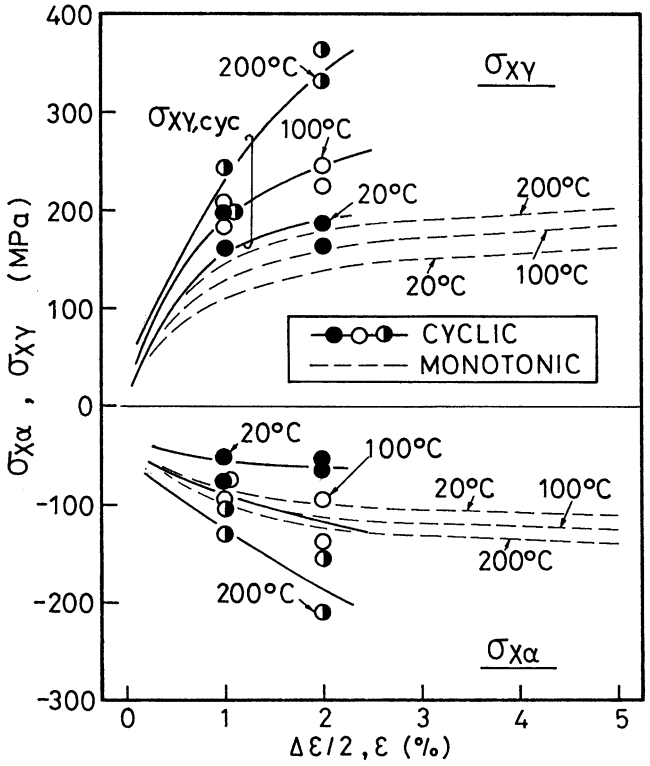

Fig. 6—X-ray internal stresses in retained austenite phase $\sigma_{X\gamma}$ and in $\alpha(\alpha_f + \alpha_b + \alpha_m)$ phase $\sigma_{X\alpha}$ of TDP steel, which is monotonically deformed to ε or cyclically deformed to $N = N_f/2$ cycles under a half-strain amplitude $\Delta\varepsilon/2$ at 20 °C, 100 °C, and 200 °C.

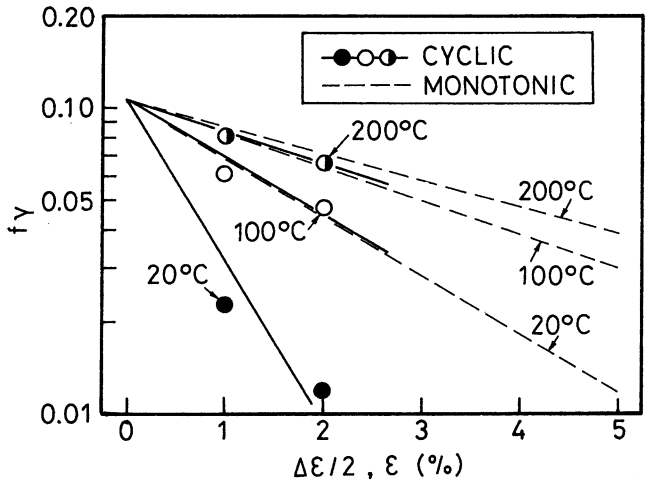

Fig. 7—Variation in retained austenite content f_γ with monotonic strain ε or a half-strain amplitude $\Delta\varepsilon/2$ for TDP steel. The number of cycles is $N = N_f/2$.

D. *Deformation-Transformation Behavior of Retained Austenite*

Figure 7 shows the variation in retained austenite content with $\Delta\varepsilon/2$ or ε in the TDP steel, which is cyclically deformed to $N = N_f/2$ cycles or is monotonically deformed. It is found that the logarithmic retained austenite content linearly decreases with $\Delta\varepsilon/2$ and ε at all the deformation temperatures,

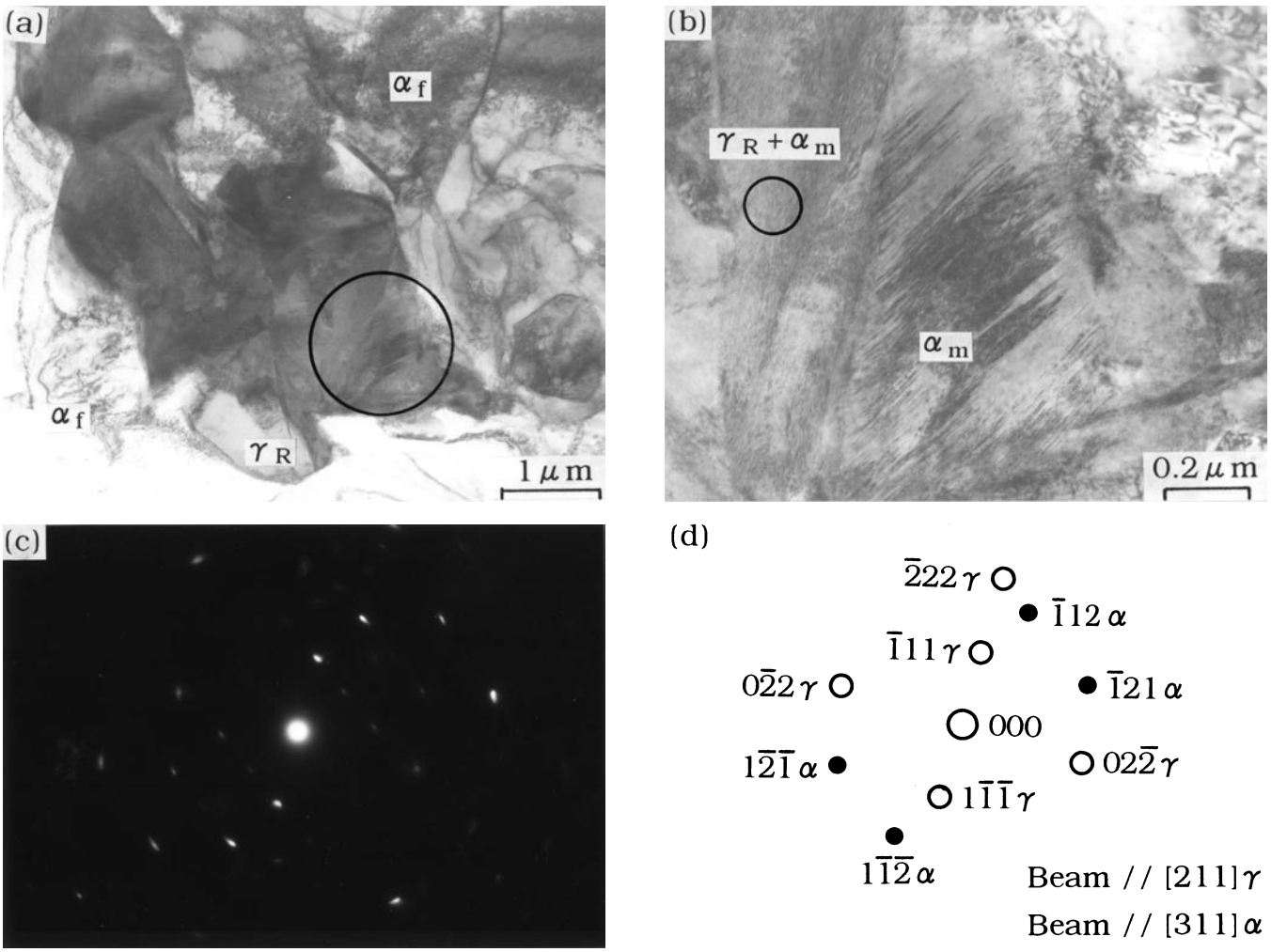

Fig. 8—Transmission electron micrographs showing strain-induced twinned martensite (α_m), untransformed retained austenite (γ_R), and untransformed retained austenite coexisting with martensite ($\gamma_R + \alpha_m$) in an original retained austenite particle of TDP steel cyclically deformed to $N = N_f/2$ at 200 °C. (*a*) Bright-field image, (*b*) high magnification of encircled area in (a), (*c*) selected area diffraction pattern of encircled area in (b), and (*d*) interpretation of diffraction pattern.

and the slope of the straight line decreases with increasing deformation temperature. When compared with monotonic deformation, cyclic deformation tends to promote the SIT of the retained austenite, in particular, at 20 °C.

Figure 8 shows a typical structure change in an original retained austenite particle of the TDP steel cyclically deformed to $N = N_f/2$ cycles at 200 °C. In the photographs, strain-induced twinned martensite films are observed in the original retained austenite particles, coexisting with the untransformed retained austenite. We verified that the strain-induced martensite occurs preferentially in large retained austenite particles, and the martensite content gradually increases with decreasing deformation temperature. A similar transformation behavior is reported in monotonic deformation.[10,11]

Many dislocations were observed in the untransformed region of the large retained austenite particles or in the small retained austenite islands during cyclic deformation. However, no deformation twin was in existence even when cyclically deformed at 200 °C, which differs from that of monotonic deformation.[2]

The increase in dislocation density in the untransformed retained austenite is also confirmed from Figure 9. Namely, the ratio of line breadth of a half-maximum X-ray intensity of strained austenite to that of an unstrained one $\Delta\theta_{X\gamma}/\Delta\theta_{X\gamma 0}$ increases with $\Delta\varepsilon/2$ and with cyclic deformation temperature.

We also observed that the cell structure is formed in the ferrite matrix of the TDP steel over all the cyclic deformation temperatures, as shown in Figure 10. The cell size is nearly equal to that of the DP steel cyclically deformed at 20 °C.

IV. DISCUSSION

In the present study, the TDP steel was found to undergo significant cyclic hardening. Also, a decrease in plastic strain amplitude was observed with an increase in deformation temperature. This behavior might be owing to (1) a long-range internal stress and (2) the SIT behavior of the retained austenite, since they particularly influence the strain hardening rate at an early stage.[9,10,11] So, at first, the contribution of the long-range internal stress to the total increment of cyclic hardening at 20 °C to 200 °C in the TDP steel was estimated. Then, the cyclic hardening behavior and hysteresis response were related with the deformation-transformation behavior and the internal stress. The forest-hardening stress (σ_f) and transformation hardening

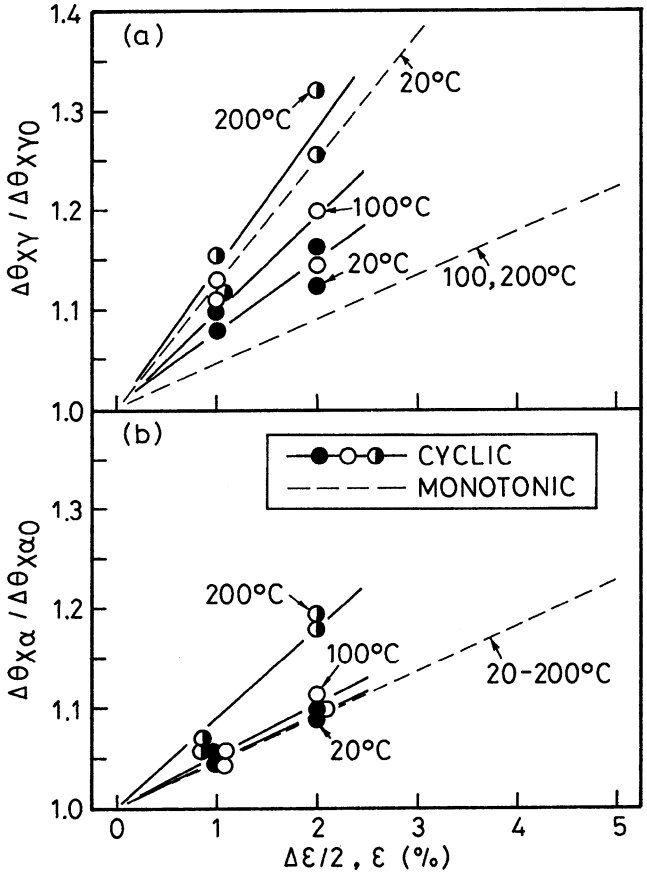

Fig. 9—Ratio of line breadth at a half-maximum X-ray intensity in (*a*) retained austenite phase $\Delta\theta_{X\gamma}/\Delta\theta_{X\gamma 0}$ or (*b*) $\alpha(\alpha_f + \alpha_b + \alpha_m)$ phase $\Delta\theta_{X\alpha}/\Delta\theta_{X\alpha 0}$ of TDP steel, which is monotonically deformed to ε or cyclically deformed to $N = N_f/2$ cycles under a half-strain amplitude $\Delta\varepsilon/2$ at 20 °C, 100 °C, and 200 °C.

stress (σ_i) were omitted in the estimation due to the complexities involved.

A. *Theory*

According to the continuum model[17,18] associated with Eshelby's theory,[19] when a two-phase alloy containing fine or grainlike second phase is plastically strained to ε in uniaxial tension, a true increment of strain hardening $\Delta\sigma_h$, as illustrated in Figure 11, is obtained from

$$\Delta\,\sigma_h(\varepsilon) = \sigma(\varepsilon) - \sigma^M(\varepsilon) \qquad [4]$$

$$= \sigma_i(\varepsilon) + \sigma_f(\varepsilon) \qquad [5]$$

where the σ and the σ^M represent the flow stresses of two-phase alloy and soft matrix, respectively. The σ_i and the σ_f are the ''*mean internal stress*'' (or long-range internal stress) resulting from unrelaxed strain ε_p^u,[20] or eigen strain,[21] and *forest-hardening stress*, proposed by Ashby,[22] respectively. And, they are given as follows:

$$\sigma_i(\varepsilon) = \{(7 - 5\,\nu)\,\mu/5(1 - \nu)\} \cdot f \cdot \varepsilon_p^u \qquad [6]$$

$$\sigma_f(\varepsilon) = \zeta\,\mu\,(\mathbf{b} \cdot f \cdot \varepsilon/2r)^{1/2} \qquad [7]$$

where μ and ν are the shear modulus and Poisson's ratio of each phase, respectively. The term ζ is a constant, f is the volume fraction of the second phase, **b** is the Burgers vector, and r denotes the mean diameter of the second-phase particles.

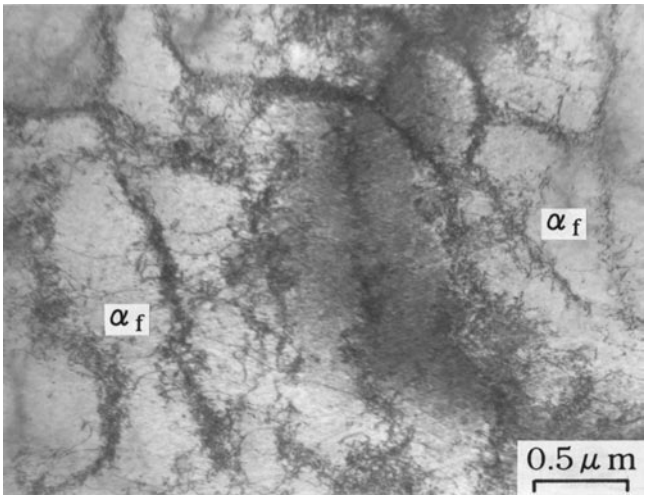

Fig. 10—Transmission electron micrograph showing the cell structure in the ferrite matrix of TDP steel cyclically deformed to $N = N_f/2$ at 200 °C.

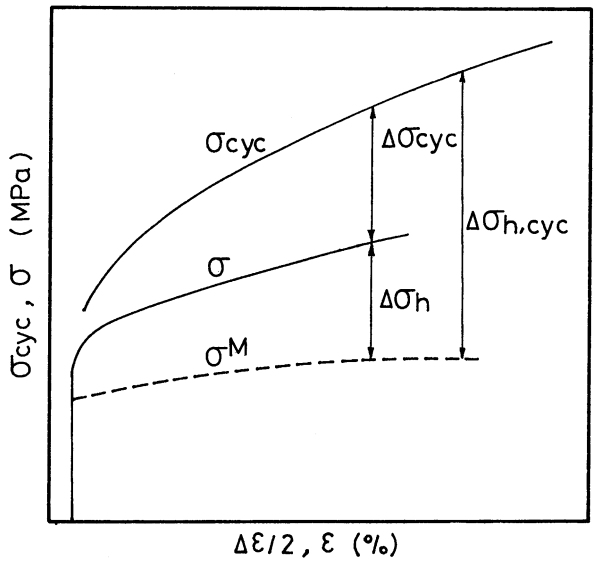

Fig. 11—Definition of $\Delta\sigma_h$ and $\Delta\sigma_{h,\mathrm{cyc}}$ at $N = N_f/2$ cycles.

When applying the preceding continuum theory to the monotonic deformation of the TDP steel, we need to consider the ''strain-induced martensite hardening'', σ_t, resulting from an increase in the strain-induced martensite content. Of course, the shear and expansion strains occurring on the SIT reduce the mean internal stress in the matrix, according to a previous research.[10,11] Thus, Eq. [5] is modified as the following equation:

$$\Delta\,\sigma_h(\varepsilon) = \sigma(\varepsilon) - \sigma^M(\varepsilon) = \sigma_i(\varepsilon) + \sigma_f(\varepsilon) + \sigma_t(\varepsilon) \qquad [8]$$

If the mean internal stress of the second phase is assumed to be equal to that of the retained austenite particles, the experimental mean internal stress σ_i^* in the matrix is estimated by substituting the X-ray internal stress $\sigma_{X\gamma}$ measured in retained austenite particles (Figure 6) into the following equation:[18,21]

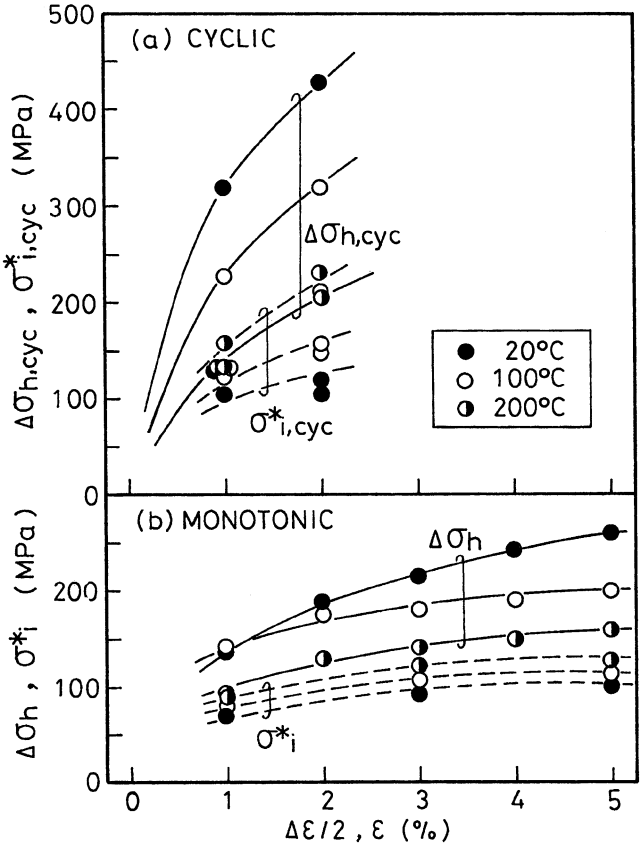

Fig. 12—Calculated values of (*a*) $\Delta\sigma_{h,cyc}$ and $\sigma^*_{i,cyc}$ at $N = N_f/2$ cycles and (*b*) $\Delta\sigma_h$ and σ^*_i at various deformation temperatures in TDP steel.

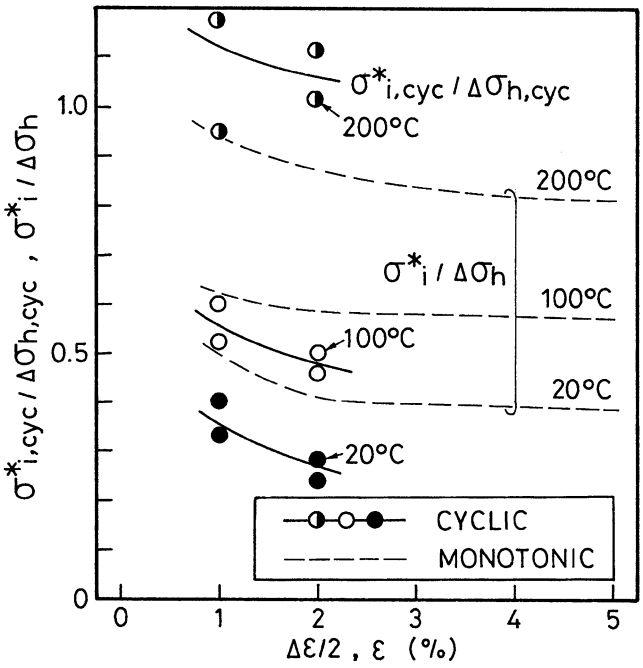

Fig. 13—Absolute values of $\sigma^*_i/\Delta\sigma_h$ and $\sigma^*_{i,cyc}/\Delta\sigma_{h,cyc}$ at various deformation temperatures in TDP steel.

$$\sigma^*_i(\varepsilon) = -3/2 \cdot f/(1-f) \cdot \sigma_{x\gamma}(\varepsilon) \quad [9]$$

If the preceding theory is applied to cyclic deformation in the same way, the total cyclic hardening increment $\Delta\sigma_{h,cyc}$ defined by the sum of $\Delta\sigma_{cyc}$ and $\Delta\sigma_h$ (Figure 11) is given as

$$\begin{aligned}\Delta\sigma_{h,cyc}(\Delta\varepsilon/2) &= \sigma_{cyc}(\Delta\varepsilon/2) - \sigma^M(\Delta\varepsilon/2) \\ &= \sigma_{i,cyc}(\Delta\varepsilon/2) + \sigma_{f,cyc}(\Delta\varepsilon/2) + \sigma_{t,cyc}(\Delta\varepsilon/2)\end{aligned} \quad [10]$$

where $\sigma_{i,cyc}$, $\sigma_{f,cyc}$, and $\sigma_{t,cyc}$ are the mean internal stress, forest-hardening stress, and strain-induced martensite hardening with respect to cyclic deformation.

Experimental mean internal stress $\sigma^*_{i,cyc}$ in the matrix at $N = N_f/2$ cycles is calculated from

$$\sigma^*_{i,cyc}(\Delta\varepsilon/2) = -3/2 \cdot f/(1-f) \cdot \sigma_{x\gamma,cyc}(\Delta\varepsilon/2) \quad [11]$$

where $\sigma_{X\gamma,cyc}$ is the X-ray internal stress of the retained austenite occurring on cyclic deformation.

B. *Contribution of Internal Stress to the Cyclic Hardening Increment*

The $\Delta\sigma_h$, σ^*_i, and $\Delta\sigma_{h,cyc}$ and $\sigma^*_{i,cyc}$ at $N = N_f/2$ cycles were calculated by substituting the measured flow stress of the TDP steel σ (Figure 3), the stress amplitude σ_{cyc} of the TDP steel (Figure 3), the X-ray internal stresses $\sigma_{X\gamma}$, $\sigma_{X\gamma,cyc}$ (Figure 6), and the volume fraction of the second-phase f (Table III) into Eqs. [8] through [11]. In Eqs. [8] and [10], the flow stress of a ferritic steel (0.006C-1.5Si-1.5Mn-0.036Al, mass pct)[9] was modified by means of the Hall–Petch equation and was substituted into the σ^M. These calculated values are shown in Figure 12. And, absolute values of $\sigma^*_i/\Delta\sigma_h$ and $\sigma^*_{i,cyc}/\Delta\sigma_{h,cyc}$ at $N = N_f/2$ cycles, which represent a contribution of the internal stress, are shown in Figure 13.

From Figure 12, it is noted that when cyclically deformed at 200 °C, the experimental mean internal stress $\sigma^*_{i,cyc}$ nearly agrees with the total cyclic hardening increment $\Delta\sigma_{h,cyc}$. Thereby, the $\sigma^*_{i,cyc}/\Delta\sigma_{h,cyc}$ value seems to be nearly equal to 1.0. A similar tendency also appears in the case of monotonic deformation at 200 °C, although the $\sigma^*_{i,cyc}/\Delta\sigma_h$ value is equal to about 0.8. Further, the SIT was considerably suppressed during cyclic deformation at 200 °C (Figure 7). In addition, the $\Delta\theta_{X\gamma}/\Delta\theta_{X\gamma 0}$ value significantly increased (Figure 9), which means that the untransformed retained austenite strain hardens during cyclic deformation. Therefore, the cyclic hardening at 200 °C may be primarily responsible for the increased compressive mean internal stress resulting from stable and strain-hardened retained austenite particles. Figures 12 and 13 also indicate that a small amount of SIT hardly lowers the mean internal stress. However, we suppose that the $\sigma^*_{i,cyc}$ is overestimated and the $\sigma_{f,cyc}$ and $\sigma_{t,cyc}$ slightly contribute to the $\Delta\sigma_{h,cyc}$.

On the other hand, when cyclically deformed at 20 °C, $\sigma^*_{i,cyc}$ becomes minimum and its contribution to the $\Delta\sigma_{h,cyc}$ is considerably decreased to $\sigma^*_{i,cyc}/\Delta\sigma_{h,cyc} = 0.2$ to 0.4, as in the case of monotonic deformation at 20 °C. According to a previous study[10,11] on monotonic deformation, a large amount of SIT of retained austenite to martensite relaxes the mean internal stresses in the ferrite matrix and in the untransformed retained austenite phase due to the local expansion and shear strains. Therefore, the strain-induced martensite hardening plays an important part in large cyclic hardening at 20 °C, accompanied with small contributions of the mean internal stress $\sigma_{i,cyc}$ (or $\sigma^*_{i,cyc}$) and the forest-hardening stress $\sigma_{f,cyc}$.

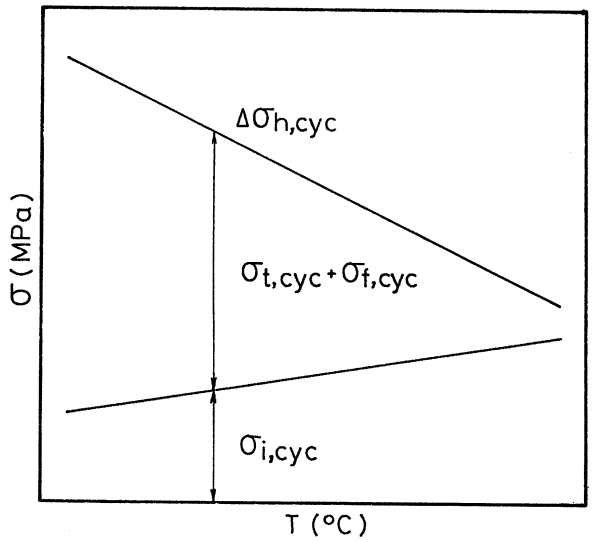

Fig. 14—Schematic contributions of mean internal stress $\sigma_{i,cyc}$, forest-hardening stress $\sigma_{f,cyc}$, and strain-induced transformation hardening stress $\sigma_{t,cyc}$ on the total cyclic hardening increment $\Delta\sigma_{h,cyc}$ in TDP steel.

From the aforementioned facts, contributions of the $\sigma_{i,cyc}$, the $\sigma_{f,cyc}$, and the $\sigma_{t,cyc}$ to the total cyclic hardening increment $\Delta\sigma_{h,cyc}$ are schematically summarized in Figure 14. At present, it is difficult to quantify the contributions of the $\sigma_{t,cyc}$ and the $\sigma_{f,cyc}$ to the $\Delta\sigma_{h,cyc}$. However, we suppose that the contribution of the $\sigma_{f,cyc}$ is very small and is negligible.

C. *Roles of Internal Stress in the Hysteresis Curve*

In the general steels, the lower the stress amplitude σ_{cyc}, the larger the plastic strain amplitude $\Delta\varepsilon_p$ becomes under constant strain amplitude. However, in the present TDP steel cyclically deformed at 100 °C and 200 °C, a contrary tendency has appeared, as shown in Figure 4. Namely, the plastic strain amplitude becomes small with the decrease in stress amplitude. The reason for this is explained as follows.

It is well known that the Young's modulus gradually decreases with the increase in deformation temperature. In the plain carbon steels, however, the Young's modulus lowers by only 10 pct, at the most, over a temperature range of 20 °C to 200 °C.[23] Thus, it is difficult to explain the large decrease in the plastic strain amplitude only by the decrease in Young's modulus.

During cyclic deformation at 100 °C and 200 °C under $\Delta\varepsilon/2 = \pm 1$ to ± 2, high $\sigma^*_{i,cyc}$ values of 100 to 200 MPa can be estimated to occur, as shown in Figure 12. These values nearly agree with the decreases in the initial flow stresses on reverse deformation. Therefore, the high negative or compressive mean internal stress occurring in the ferrite matrix may effectively lower the initial reverse flow stress σ_R and, as a result, reduce the apparent Young's modulus or plastic strain amplitude at 100 °C and 200 °C.

V. CONCLUSIONS

1. The Cyclic deformation behavior of the TDP steel was characterized by the large initial cyclic hardening and the successive small hardening or softening, similar to the DP steel. With an increasing deformation temperature and retained austenite stability against the SIT, the cyclic hardening became smaller, with concomitant decreases in cyclic stress amplitude and plastic strain amplitude.
2. Stable retained austenite, as a hard phase, effectively enhanced a long-range compressive internal stress in the ferrite matrix. On the other hand, strain-induced martensite relaxed the internal stresses in the retained austenite and the matrix by local expansion and shear strains.
3. Large cyclic hardening at 20 °C may be primarily controlled by strain-induced martensite hardening, accompanied by small contributions of long-range internal stress and forest-hardening stress. On the other hand, small cyclic hardening and the decreased plastic strain amplitude at 100 °C and 200 °C were caused by the high long-range internal stress resulting from the stable and strain-hardened retained austenite particles.

ACKNOWLEDGMENT

The authors thank the Kawasaki Steel 21st Century Foundation (Tokyo, Japan) for financial support.

REFERENCES

1. O. Matsumura, Y. Sakuma, and H. Takechi: *Iron Steel Inst. Jpn.*, 1987, vol. 27, pp. 570-79.
2. K. Sugimoto. M. Kobayashi, and S. Hashimoto: *Metall. Trans. A.* 1992. vol. 23A, pp. 3085-91.
3. K. Sugimoto, N. Usui, M. Kobayashi, and S. Hashimoto: *Iron Steel Inst. Jpn. Int.*, 1992, vol. 32, pp. 1311-18.
4. K. Sugimoto, M. Misu, M. Kobayashi, and H. Shirasawa: *Iron Steel Inst. Jpn. Int.*, 1993, vol. 33, pp. 775-82.
5. Y. Sakuma, D.K. Matlock, and G. Krauss: *Metall. Trans. A*, 1992, vol. 23A, pp. 1233-41.
6. K. Sugimoto, M. Kobayashi, A. Nagasaka, and S. Hashimoto: *Iron Steel Inst. Jpn. Int.*, 1995, vol. 35, pp. 1407-14.
7. A. Itami, M. Takahashi, and K. Ushioda: *Proc. Symp. on High-Strength Sheet Steels for the Automotive Industry*, R. Pradhan, ed., AIME, Baltimore, MD, 1994, pp. 245-54.
8. V.F. Zackay, E.R. Parker, D. Fahr, and R. Bush: *Trans. ASM*, 1967, vol. 60, pp. 252-59.
9. S. Yasuki, K. Sugimoto, M. Kobayashi, and S. Hashimoto: *J. Jpn. Inst. Met.*, 1990, vol. 54, pp. 1350-57.
10. K. Sugimoto, M. Kobayashi, S. Yasuki, and S. Hashimoto: *Mater. Trans. JIM*, 1995, vol. 36, pp. 632-38.
11. K. Sugimoto, M. Kobayashi, H. Matsushima, and S. Hashimoto: *Trans. Jpn. Soc. Mech. Eng. A*, 1995, vol. 61-581, pp. 80-86.
12. H. Maruyama: *J. Jpn. Soc. Heat Treatment*, 1977, vol. 17, pp. 198-204.
13. Z. Nishiyama: *Martensite Transformation*, Maruzen, Tokyo, 1979, p. 13.
14. G.R. Speich, V.A. Demarest, and R.L. Miller: *Metall. Trans. A*, 1981, vol. 12A, pp. 1419-28.
15. *Society of Materials Science Japan: Standard Measurement Method of X-Ray Stress*, SMSJ, Kyoto, 1977, pp. 3-9.
16. M. Mizui, H. Takechi, and T. Sekine: *J. Iron Steel Inst. Jpn.*, 1990, vol. 76, pp. 414-21.
17. Y.W. Chang and R.J. Asaro: *Met. Sci.*, 1978, vol. 12, pp. 277-84.
18. M.T. Ma, B.Z. Sun, and Y. Tomota: *Iron Steel Inst. Jpn. Int.*, 1989, vol. 29, pp. 74-77.
19. J.D. Eshelby: *Proc. R. Soc., Ser. A*, 1957, vol. A241, pp. 376-96.
20. J.D. Atkinson, L.M. Brown, and W.M. Stobbs: *Phil. Mag.*, 1974, vol. 30, pp. 1247-80.
21. T. Mura and T. Mori: *Micromechanics*, Baifu-Kan, Tokyo, 1976.
22. M.F. Ashby: *Phil. Mag.*, 1966, vol. 14, pp. 1157-78.
23. *Japan Society of Mechanical Engineers: The Modulus of Elasticity of Metals and Alloys*, JSME, Tokyo, 1980, pp. 18-20.